


Analysis of thermal characteristics with multi-physics coupling for the feed system of a precision CNC machine tool

Junjian ZHENG¹, Xiaolei DENG^{2*}, Junshou YANG², Wanjun ZHANG², Xiaoliang LIN², Shaofei JIANG¹, Xinhua YAO³, and Hongyao SHEN³

¹ College of Mechanical Engineering, Zhejiang University of Technology, Hangzhou 310023, China

² Key Laboratory of Air-driven Equipment Technology of Zhejiang Province, Quzhou University, Quzhou 324000, China

³ School of Mechanical Engineering, Key Laboratory of 3D Printing Process and Equipment of Zhejiang Province, State Key Laboratory of Fluid Power and Mechatronic Systems, Zhejiang University, Hangzhou 310027, China

Abstract. The machining accuracy of CNC machine tools is significantly affected by the thermal deformation of the feed system. The ball screw feed system is extensively used as a transmission component in precise CNC machine tools, responsible for converting rotational motion into linear motion or converting torque into repetitive axial force. This study presents a multi-physical coupling analysis model for the ball screw feed system, considering internal thermal generation, intending to reduce the influence of screw-induced thermal deformation on machining accuracy. This model utilizes the Fourier thermal conduction law and the principle of energy conservation. By performing calculations, the thermal source and thermal transfer coefficient of the ball screw feed system are determined. Moreover, the thermal characteristics of the ball screw feed system are effectively analyzed through the utilization of finite element analysis. To validate the proposed analysis model for the ball screw feed system, a dedicated test platform is designed and constructed specifically to investigate the thermal characteristics of the ball screw feed system in CNC machine tools. By selecting specific CNC machine tools as the subjects of investigation, a comprehensive study is conducted on the thermal characteristics of the ball screw feed system. The analysis entails evaluating parameters like temperature field distribution, thermal deformation, thermal stress, and thermal equilibrium state of the ball screw feed system. By comparing the simulation results from the analysis model with the experimental test results, the study yields the following findings: The maximum absolute error between the simulated and experimental temperatures at each measuring point of the feed system components is 2.4°C, with a maximum relative error of 8.7%. The maximum absolute error between the simulated and experimental temperatures at the measuring point on the lead screw is 2.0°C, with a maximum relative error of 6.8%. The thermal characteristics obtained from the steady-state thermal analysis model of the feed system exhibit a prominent level of agreement with the experimental results. The research outcomes presented in this paper provide valuable insights for the development of ball screw feed systems and offer guidance for the thermal design of machine tools.

Keywords: CNC machine tool; ball screw; feed system; module; thermal state characteristics; multiple physical field coupling; contactless.

1. INTRODUCTION

Establishing the accuracy of CNC machine tools heavily relies on the thermal characteristics of the feed system. Among the frequently employed elements for the feed system in machine tools, the ball screw occupies a prominent position. As a key component, the thermal deviation resulting from thermal deformation in the ball screw is frequently the main contributor to the positioning error of the feed system, thereby directly influencing the overall precision of the machine tool [1].

Currently, Chinese, and foreign scholars are dedicating their research efforts to studying the modeling of thermal characteristics and thermal errors in ball screw feed systems. Machine modelling and simulation is the use of models as a framework

for simulation to develop the data used to make technical decisions, in the field of mechanical engineering. Modelling and simulation reduce costs, improve the product and system quality, and document any conclusions drawn. Additionally, models can be updated and improved using the results from real-world experiments [2]. In a study conducted by Li *et al.* [3], they utilized a combination of the finite element method and the Monte Carlo method to investigate this area. Moreover, they proposed an adaptive real-time model (ARTM) that demonstrates remarkable effectiveness in predicting the transient distribution of temperature fields and thermal errors in ball screws. This model ensures accurate estimation of thermal characteristics in real time. Additionally, Li developed a numerical prediction algorithm specifically designed for analyzing the thermal characteristics of spiral shafts. The effectiveness of this algorithm was then validated through experimental testing. Based on an analysis of thermal generation and thermal transfer in the ball screw system, Yang *et al.* [4] established a mathematical model to describe the axial thermal expansion of the ball screw. This model was devel-

*e-mail: dxl@zju.edu.cn

Manuscript submitted 2023-11-03, revised 2023-12-28, initially accepted for publication 2023-12-29, published in March 2024.

oped to accurately predict the thermal expansion phenomenon. To verify the efficacy of the model, Yang conducted experiments that confirmed its accuracy and reliability. Ma *et al.* [5] put forth a prediction model for the contact thermal conductivity (TCC) of solid joints. This model was developed by considering the rough surface microstructure description and contact load distribution of the joints. Furthermore, Ma successfully enhanced the precision of simulating the thermal characteristics of the ball screw feed system by developing a dynamic thermal-structure coupling model that accounted for the influence of thermal contact conductance (TCC) on the accuracy of simulation results. In order to examine the thermal deformation of ball screws, Xia *et al.* [6] developed a dynamic characteristic analysis model that employed the least square system identification theory. Furthermore, they conducted an analysis to evaluate the impact of varying thermal sources on the one-dimensional thermal transfer in ball screws. The objective of this study was to gain insights into how changing thermal sources affect the thermal transfer process, ultimately influencing the thermal deformation of the ball screw. In Liang's research [7], the finite element method was employed to examine the thermal characteristics of the Y-type feed system in a particular gantry machine tool. By utilizing this approach, valuable insights regarding the thermal behavior of the system were gained. To ensure the accuracy and reliability of their findings, Liang conducted experiments and compared the results with those obtained from the finite element analysis model. The experimental verification successfully confirmed the effectiveness of the finite element analysis model in accurately predicting the thermal characteristics of the Y-type feed system. Su *et al.* [8] introduced a thermal error modeling method for the ball screw feed system, utilizing the finite element method. They incorporated a dynamic approach by altering the grid distribution at different time steps in the finite element simulation. This allowed them to accurately simulate the thermal source movement at the screw nut within the model. To validate the accuracy and effectiveness of the proposed model, Su conducted experimental tests under various working conditions. The experimental results confirmed the model accuracy and demonstrated its effectiveness in predicting thermal errors in the ball screw feed system. ZAPLATA [9] constructed a dedicated test platform for a ball screw assembly that included an integrated temperature sensor. The primary objective of this setup was to assess the reliability and accuracy of infrared measurement techniques when applied to ball screws. By conducting experiments on the test platform, ZAPLATA aimed to provide empirical evidence regarding the effectiveness and trustworthiness of using infrared measurement methods in the context of ball screw applications. Li *et al.* [10] integrated stochastic theory, genetic algorithm, and radial basis function neural network to develop an inverse stochastic model capable of predicting thermal errors in a system. This innovative approach considers the inherent randomness of various influencing factors. By combining these methodologies, Li aimed to accurately estimate thermal errors by considering the probabilistic nature of the system. The proposed model provides a comprehensive framework for predicting and mitigating thermal errors while accounting for the uncertainties associated with in-

fluencing factors. Deng *et al.* [11, 12] constructed a multi-source heterogeneous acquisition test platform, incorporating diverse types of sensors, to capture diverse types of information and signals during the operation of CNC machine tools. After fusing the collected data, Deng applied the multi-source heterogeneous information to thermal error modeling. To optimize the selection of temperature key points in thermal error modeling for different CNC machine tools, a novel approach was proposed. This method effectively reduces the number of temperature measurement points while enhancing the accuracy of thermal error prediction. Experimental studies conducted on multiple machine tools validated the efficacy of this approach in improving the accuracy of thermal error models while significantly reducing the number of required sensors. A. Oyanguren *et al.* [13] introduced a numerical simulation method for determining the preload of a double-nut ball screw using the three-dimensional finite element method. By employing this approach, they were able to analyze and quantify the changes in preload as a result of temperature elevation within the ball screw system. To validate the obtained results, experiments were conducted under diverse initial conditions. The experimental findings confirmed the accuracy and reliability of the numerical simulation method proposed by A. Oyanguren in predicting the variation of preload with temperature rise in the double-nut ball screw system. Shi *et al.* [14] developed a mathematical model for the axial thermal expansion of the ball screw by analyzing the thermal generation and thermal transfer within the ball screw system. Regression analysis was employed to characterize the thermal error observed in experimental data. Ultimately, the accuracy and effectiveness of the proposed approach were validated through experimental verification.

This study introduces a comprehensive three-dimensional analysis model for the ball screw feed system, incorporating Fourier's thermal conduction law and principles of energy conservation. This research aims to examine the thermal characteristics of the feed system in an NC machine tool by conducting comprehensive analysis and calculations on the thermal source and thermal transfer coefficient of the ball screw system under different operational conditions. The temperature distribution, thermal deformation, thermal stress, and thermal equilibrium state of the feed system are determined using finite element analysis. Furthermore, an experimental setup is designed and constructed to validate the accuracy of the analysis model and investigate the thermal properties of the feed system in the NC machine tool. Through a case study on a specific machine tool's feed system, the efficacy of the proposed analysis model is successfully verified. The findings of this study offer valuable insights for the future thermal design of CNC machine tools and the enhancement of machining precision.

2. MULTIPHYSICS COUPLING MODEL

2.1. Fluid-temperature field coupling model

In the ball screw feed system, thermal generation primarily arises from three sources: power loss in the motor, friction between the screw and nut pair, and friction within the bearings. The amount

of thermal generated by friction is influenced by factors such as the feed rate, lubrication method, and assembly conditions, all of which impact the temperature distribution along the ball screw.

However, directly measuring the temperature of the ball screw and screw nut pair can be challenging, often necessitating the use of numerical simulations to determine the temperature distribution along the ball screw. In this particular study, a combination of non-contact thermal imaging measurement techniques and computer simulation is utilized to analyze the temperature field of the ball screw. By integrating these methods, a more comprehensive understanding of the temperature distribution can be achieved.

The finite element method is employed to calculate the temperature distribution of the ball screw based on the following assumptions [15–17].

1. The thermal generated by the reciprocating motion of the screw nut through friction is uniformly distributed, and a constant proportion of the generated thermal is transferred to the screw.
2. When the temperature increase is small, thermal radiation can be disregarded.
3. The thermal transfer between the solid structure and the lubricant can be assumed to be negligible.
4. The convective thermal transfer coefficient remains constant when the same feed quantity is in motion.
5. The lead screw nut and the bearing are simplified as hollow cylinders, while the lead screw is simplified as a solid cylinder with a uniform thermal production rate. Furthermore, the small structures within the ball screw system, such as chamfering, rounded corners, threaded holes, and keyways, can be reasonably simplified.

2.1.1. Differential equation of thermal conduction in the feed system

By applying Fourier's law of thermal conductivity and the law of conservation of energy, we can derive the thermal conduction differential equation for a three-dimensional steady-state temperature field with an internal thermal source [18] as follows:

$$\frac{\partial^2 T}{\partial x^2} + \frac{\partial^2 T}{\partial y^2} + \frac{\partial^2 T}{\partial z^2} + \frac{q_v'''}{\lambda} = 0, \quad (1)$$

where: $T = f(x, y, z)$ represents the temperature field distribution function related to position, λ represents the thermal conductivity of the material, q_v''' represents the intensity of the internal thermal source, and x, y, z represents the Cartesian coordinate.

2.1.2. The governing equations for fluid flow

The control equations for fluid flow can be divided into the mass conservation equation, momentum conservation equation, and energy conservation equation which are respectively expressed as [19]:

$$\begin{cases} \frac{\partial \rho}{\partial t} + \nabla \cdot (\rho v) = 0, \\ \rho \left(\frac{\partial v}{\partial t} + v \cdot \nabla v \right) = -\nabla p + \mu \nabla^2 v + \rho g, \\ \rho C \left(\frac{\partial T}{\partial t} + v \cdot \nabla T \right) = \nabla \cdot (k \nabla T) + Q, \end{cases} \quad (2)$$

where: ρ represents the fluid density, v represents the fluid velocity, t represents the time, p represents the pressure of the fluid, μ represents the kinematic viscosity of the fluid, g represents the acceleration of gravity, C represents the specific thermal capacity of the fluid, T represents the temperature of the fluid, k represents the thermal conductivity of the fluid, and Q represents the thermal input to the fluid per unit volume per unit time.

2.1.3. Thermal source calculation

A. Thermal flux calculation of servo motor

The thermal flux of the motor Q_m [20] is:

$$Q_m = a \left(\frac{M_m n}{9550} \right) (1 - \eta), \quad (3)$$

where: η represents the working efficiency of the servo motor, M_m represents the output torque, its units are N·m, n represents the servo motor speed, its units are r/min, and a represents the thermal correction factor of the servo motor, which is usually equal to 0.3.

B. Thermal flux calculation of ball screw nut pair

The formula for calculating the thermal flux of the ball screw nut pair Q_n is as follows [21]:

$$Q_n = \frac{2\pi}{60} M n, \quad (4)$$

where: n represents the speed of the ball screw, its units are r/min and M is the friction torque of the ball screw pair, its units are N·m. The calculation formula for the friction torque is as follows [22]:

$$M = 2z (M_e + M_g) \cos \beta, \quad (5)$$

where: z is the number of rolling elements, M_e is the friction resistance moment, and M_g is the cumulative sliding friction torque. β is the spiral Angle of the ball screw raceway.

$$M_e = m_\beta \sqrt[3]{\frac{4F_r^4}{v \sum r}}, \quad (6)$$

$$M_g = 0.08 \frac{f \cdot m_\alpha^2}{R} \sqrt[3]{\frac{16F_r^5}{(v \sum r)^2}}, \quad (7)$$

$$v = \frac{8}{3 \left(\frac{1-p_1^2}{E_1} + \frac{1-p_2^2}{E_2} \right)}, \quad (8)$$

where: m_α and m_β represent the coefficients related to the eccentricity of the spherical contact deformation ellipse, F_r denotes the radial pressure on a single sphere, f is the sliding

friction coefficient, p_1 and p_2 are the Poisson's ratios of the ball and raceway, E_1 and E_2 stand for Young's moduli of the ball and raceway, and $\sum r$ represents the radius of curvature, and R represents the radius of the screw [21].

C. Thermal flux calculation of bearing

According to Harris's theory, the calculation for the bearing thermal flux Q_b can be expressed as follows [9, 21]:

$$Q_b = 1.047 \times 10^{-4} n_b M_b, \quad (9)$$

$$M_b = M_1 + M_v, \quad (10)$$

where: n_b is the speed of the lead screw, M_b is the total friction torque of the bearing, M_1 is the friction torque caused by the applied load, and M_v is the friction torque caused by viscous friction.

The friction torque caused by the applied load M_1 can be calculated by the following formula [9, 21]:

$$M_1 = f_1 \cdot F_\beta \cdot d_m, \quad (11)$$

$$F_\beta = \max(0.9F_a/\tan\alpha - 0.1F_r, F_r), \quad (12)$$

where: f_1 is the coefficient related to bearing type and load, F_β is the equivalent load applied to the bearing, d_m is the pitch circle diameter of the bearing, F_a and F_r are the axial load and radial load borne by the bearing, respectively, and α is the contact angle of the bearing.

The friction torque caused by viscous friction M_v can be calculated by the following formula [9, 21]:

$$\begin{cases} M_v = 10^{-7} \cdot f_0 \cdot (\nu_0 n)^{2/3} \cdot d_m^3 & \nu_0 n \geq 2000, \\ M_v = 160 \cdot 10^{-7} \cdot f_0 \cdot d_m^3 & \nu_0 n < 2000, \end{cases} \quad (13)$$

where: f_0 is the coefficient related to bearing type and lubrication method, and ν_0 is the kinematic viscosity of the lubricating oil at the operating temperature of the bearing.

2.1.4. Calculation of thermal transfer coefficient

A. Convective thermal transfer coefficient between lead screw and air

The convective thermal transfer coefficient between the lead screw and the surrounding air can be calculated using the following formula [22, 23]:

$$h = \frac{\text{Nu} \cdot \lambda_{\text{air}}}{L}, \quad (14)$$

where: Nu represents the Nusselt number, L denotes the characteristic length, and λ_{air} signifies the thermal conductivity of the ambient air.

From equation (14), it is evident that the convective thermal transfer coefficient between the lead screw and the air can be computed once the Nusselt number, represented by Nu, is determined. The calculation of the Nusselt number varies for natural convection thermal transfer and forced convection thermal transfer, employing different algorithms.

During the operation of the feed system, the rapid rotation of the lead screw intensifies the thermal exchange and convection between the lead screw and the surrounding air, leading to forced convection thermal transfer. The Nusselt number, denoted as Nu, is defined according to the following equation [10]:

$$\text{Nu} = 0.133 \text{Re}^{2/3} \text{Pr}^{1/3}, \quad (15)$$

$$\text{Re} = \frac{\omega \cdot d_m^2}{\nu}, \quad (16)$$

where: Re represents the Reynolds number, Pr denotes the Prandtl number, ω signifies the angular speed of the screw shaft, and ν represents the kinematic viscosity of air.

B. Convective thermal transfer coefficient between other components and air

The thermal exchange between the remaining components of the feed system and the surrounding air takes place through natural convection thermal transfer. The Nusselt number, denoted as Nu, can be defined in the following manner [23]:

$$\text{Nu} = C(\text{Gr} \cdot \text{Pr})^{1/4}, \quad (17)$$

$$\text{Gr} = \frac{g \cdot \beta \cdot L^3 \cdot \Delta T}{\nu^2}, \quad (18)$$

where: C is the constant associated with the flow pattern and thermal source when the heat exchange surface is vertical plane and horizontal plane, C is 0.59 and 0.54, respectively. Gr represents the Grashof number, g represents the gravitational acceleration, β represents the expansion coefficient of air, and ΔT represents the temperature difference between the ball screw feed system and the air.

2.2. Temperature-structure field coupling model

According to the theory of linear thermal stress, the total strain of an elemental body is composed of two parts: one part is caused by temperature changes, and the other part is caused by stress. The generalized Hooke's law for plane stress [24], which expresses strain in terms of thermal stress and temperature changes caused by stress, is:

$$\begin{cases} \varepsilon_x = \frac{1}{E} [\sigma_x - \mu(\sigma_y + \sigma_z)] + \alpha \Delta T, \\ \varepsilon_y = \frac{1}{E} [\sigma_y - \mu(\sigma_x + \sigma_z)] + \alpha \Delta T, \\ \varepsilon_z = \frac{1}{E} [\sigma_z - \mu(\sigma_y + \sigma_x)] + \alpha \Delta T, \\ \gamma_{xy} = \tau_{xy}/G, \quad \gamma_{yz} = \tau_{yz}/G, \quad \gamma_{xz} = \tau_{xz}/G, \end{cases} \quad (19)$$

where: ε_x , ε_y , ε_z , γ_{xy} , γ_{yz} , γ_{xz} represent the strains in the x -direction, y -direction, z -direction, and shear strain, respectively. σ_x , σ_y , σ_z represent the thermal stresses in the x -direction, y -direction, and z -direction, respectively. τ_{xy} , τ_{yz} , τ_{xz} represent the thermal stresses in the x - y plane, y - z plane, and x - z plane, respectively. μ , E , α and G represent the Poisson's ratio, elastic

modulus, coefficient of thermal expansion, and shear modulus of the material, respectively. Δt represents the temperature change.

Based on equation (19) generalized Hooke's law and elastic mechanics theory, the equilibrium differential equation (displacement equation) of thermoelasticity expressed by displacement component and the deformation continuity equation (coordination equation) expressed by stress component of thermoelasticity can be obtained. The thermal deformation and thermal stress caused by the temperature change of the feed system can be calculated according to the displacement equation and the coordination equation respectively [25].

The finite element equations for thermo-structural coupled deformation [24] are as follows:

$$\begin{bmatrix} 0 & 0 \\ 0 & C \end{bmatrix} \begin{bmatrix} \dot{\mu} \\ \dot{T} \end{bmatrix} + \begin{bmatrix} K & 0 \\ 0 & K^T \end{bmatrix} \begin{bmatrix} \mu \\ T \end{bmatrix} = \begin{bmatrix} F \\ Q \end{bmatrix}, \quad (20)$$

where: C represents the heat capacity matrix, μ represents the nodal displacement vector, $\dot{\mu}$ represents the nodal velocity vector, K represents the stiffness matrix, F represents the force vector, and Q includes the applied nodal forces and the forces caused by thermal deformation.

Based on the above theory, the heat generated by each heat source and the convective heat transfer coefficient between the surface and the air of each component are calculated by formulas (3) to (18). Then, the temperature field, thermal deformation, and thermal stress of the feed system are simulated by the finite element method based on the results obtained from the boundary condition equation, thermal conduction differential equation (1), fluid control equation (2), and thermodynamic coupling model (19), (20).

3. COUPLING EXAMPLE ANALYSIS OF FEED SYSTEM

3.1. Global analysis model

The research object chosen for this study is the RP-41 CNC machine tool ball screw feed system developed by a machine tool factory located in Hangzhou, as shown in Fig. 1. The ball screw feed system comprises several essential components, including a table, ball screw (consisting of a screw nut and screw), motor, bearings, and bed saddle. The ball screw adopts a support form with one end fixed and one end moving. The lead screw material

is GCr15, the guide rail material is 45 steel, the bearing material is Cr15Mo, and the bed saddle material is HT250. According to the literature [26], the motor is a complex composed of a variety of materials, and the material characteristics of the motor are estimated according to the characteristics of each material and its approximate proportion in the motor. The main attributes [27] are shown in Table 1.

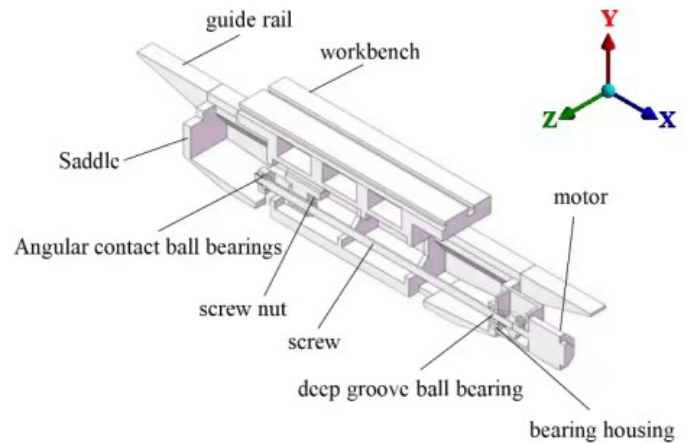


Fig. 1. Schematic diagram of ball screw feed system structure

3.2. Boundary condition result

Through formulas (3) to (18), the convective heat transfer coefficient between the surface and the air of each component in the feed system and the heat generated by each heat source can be calculated. The thermal transfer occurring between the table, bed saddle, guide rail assembly, and surrounding air in the ball screw feed system is classified as natural convection thermal transfer. The convective thermal transfer coefficient for this process can be referred to in Tables 2–4, while the outcomes of calculating other boundary conditions are presented in Tables 5–8.

Table 2

Thermal transfer coefficients of each surface and air of the table

Plane position	Top	Front and back	flank
$h/(W \cdot m^{-2} \cdot K^{-1})$	16.3	13.2	12.6

Table 1

Material properties of main components

Unit	Materials	Density ($kg \cdot m^{-3}$)	Poisson's ratio	Coefficient of linear expansion (10^{-5})	Thermal conductivity ($W \cdot m^{-1} \cdot K^{-1}$)	Young's modulus ($10^5 MPa$)
Ball screw	GCr15	7830	0.3	1.2	44	2.19
Saddle	HT250	7280	0.156	0.82	45	1.38
Rail	45 steel	7890	0.269	1.17	48	2.09
Bearing	Cr15Mo	7880	0.284	1.34	44	2.12
Motor	Multi-material complex	3950	0.28	0.5	100	0.5

Table 3

Thermal transfer coefficient between saddle and air

Plane position	Front and back	flank
$h/(W \cdot m^{-2} \cdot K^{-1})$	15.3	12.8

Table 4

Thermal transfer coefficient of each surface and air of guide rail

Plane position	Top and under	flank
$h/(W \cdot m^{-2} \cdot K^{-1})$	14.3	13.5

Table 5

Thermal transfer coefficient of lead screw surface and air at each speed

Rotational speed	3000 r/min	4000 r/min	6000 r/min
$h/(W \cdot m^{-2} \cdot K^{-1})$	26.4	32.0	41.7

Table 6

Thermal flux value of motor at each speed

Rotational speed	3000 r/min	4000 r/min	6000 r/min
Thermal flux /W	9.6	14.7	21.6

Table 7

Bearing thermal flux value at each speed

Rotational speed	3000 r/min	4000 r/min	6000 r/min
Thermal flux of angular contact bearings / W	1.2	2.3	3.7
Thermal flux of deep groove ball bearing / W	2.6	3.6	5.5

Table 8

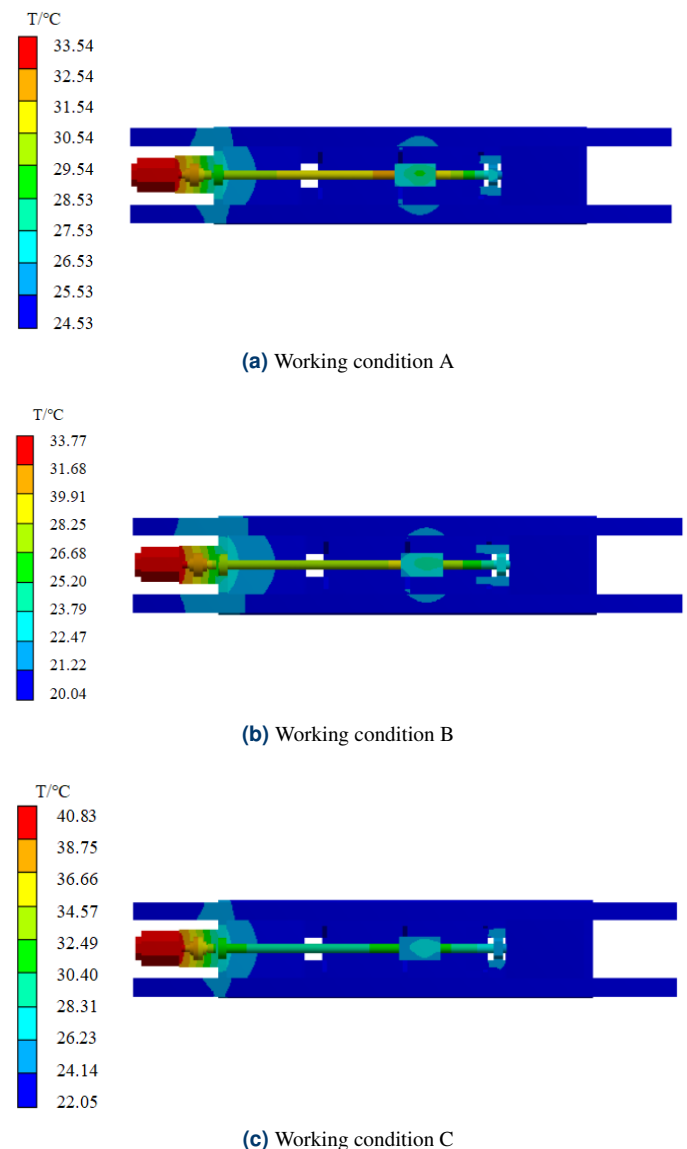
Thermal flux value of screw nut pair at each speed

Rotational speed	3000 r/min	4000 r/min	6000 r/min
Thermal flux / W	33.8	36.1	41.5

3.3. Simulation analysis of fluid-temperature field coupling

First, the three-dimensional model of the ball screw system was established with SolidWorks software, and then the model was imported into Ansys. In the simulation process, after increasing the mesh density many times, the calculation results do not change significantly. This result is used as the final simulation result in this paper. The parts of varied sizes were divided by reasonable mesh size and division method, and a total of 896 116 nodes and 492 545 grids were generated. Three working conditions A: 3000 mm/min feed rate of 200 mm stroke, B: 4000 mm/min feed rate of 200 mm stroke, and C: 6000 mm/min feed rate of 400 mm stroke were selected

for analysis. The ambient temperature under the three working conditions is 24.5°C, 20.0°C, and 22.0°C, respectively. Among them, working conditions A and C are two typical working conditions of minimum feed rate, minimum stroke, and maximum feed rate and maximum stroke, respectively. In condition B, the feed rate and stroke size are between the two. The steady-state thermal finite element simulation of three working conditions is completed by applying corresponding boundary conditions. The simulation model of the ball screw feed system was used to conduct a steady-state analysis, resulting in a contour plot illustrating the distribution of the overall temperature field and its components are shown in Figs. 2–5. According to the results, the highest temperature of the feed system appears on the upper surface of the motor housing, and its temperature value is about 33.5°C, 33.7°C, and 40.6°C, respectively, under the three working conditions of A, B, and C, and the temperature rise is about 9°C, 13.7°C, and 18.6°C, respectively. In other parts except for the motor, the highest temperature appears at the screw nut,

**Fig. 2.** Contour plot of temperature field distribution in the feed system

Analysis of thermal characteristics with multi-physics coupling for the feed system of a precision CNC machine tool

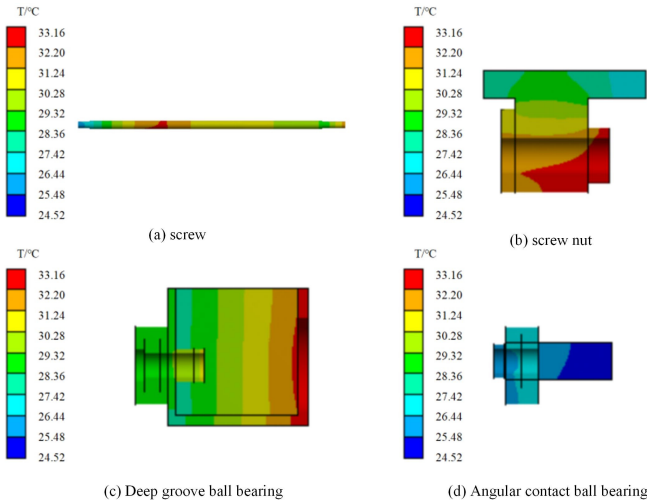


Fig. 3. Contour plot of temperature field distribution of system components (Working condition A)

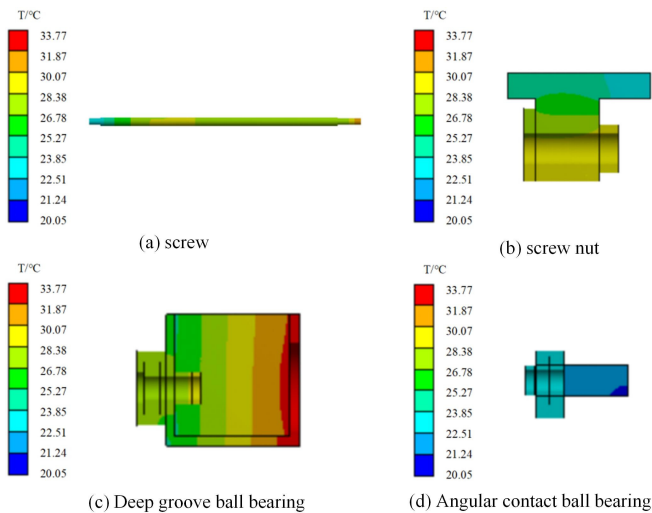


Fig. 4. Contour plot of temperature field distribution of system components (Working condition B)

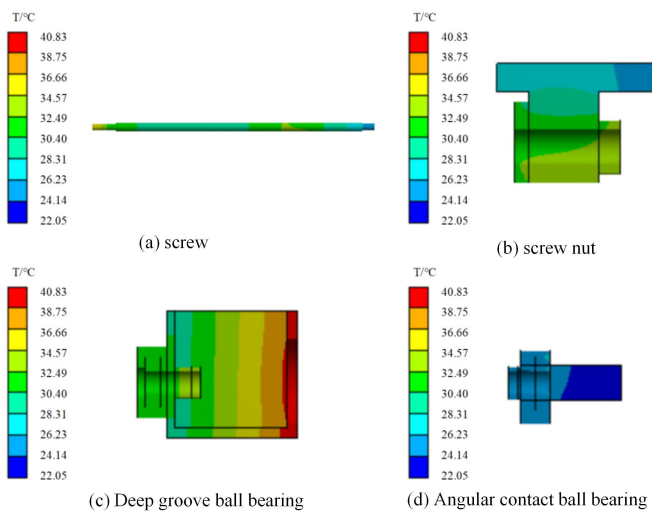


Fig. 5. Contour plot of temperature field distribution of system components (Working condition C)

whose temperature value is about 30.7°C, 27.4°C and 31.4°C under the three working conditions of A, B, and C, and the temperature rise is about 6.2°C, 7.4°C, and 9.4°C, respectively.

3.4. Simulation analysis of temperature-structure field coupling

In this study, we specifically analyze the impact of thermal deformation on working condition C, which is highly susceptible to such effects. To establish the temperature boundary condition for the ball screw feed system under operating condition C, we utilize the temperature field distribution derived from the previous section. Additionally, we account for the displacement constraint conditions among the feed system components and consider the influence of gravity. This leads us to conduct a coupled analysis that encompasses both the temperature and structural fields of the feed system. By integrating these factors, we aim to achieve a comprehensive understanding of the interaction between temperature and structural behavior within the feed system.

The axial deformation of the ball screw system has a direct influence on the machining accuracy of the machine tool. It encompasses various forms of deformation, including axial compression deformation of the lead screw, deformation at the bearing contact points, screw nut contact deformation, screw torsion deformation, and axial deformation of the support seat and nut seat. Among these, the axial deformation of the lead screw contributes significantly to the overall deformation, as highlighted in reference [28]. Figure 6 presents a thermal deformation diagram depicting the nodal points along the axis of the lead screw. At the deep groove ball bearing installation end of the lead screw, the maximum axial deformation occurs. The X-directional axial thermal deformation is approximately 11.6 μm, while the deformations in the other two directions are smaller compared to the X-directional thermal deformation.

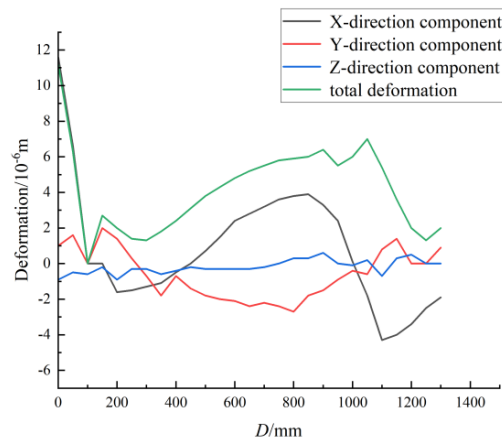


Fig. 6. Axis direction deformation of the screw

Figure 7 displays the von Mises equivalent stress distribution contour map of the lead screw. Without considering the machining of the workpiece, the stress changes in the feed system were mainly caused by thermal deformation and displacement constraints, so the stress concentration of the feed system ap-

peared at the installation of the deep groove ball bearing, and the maximum von Mises equivalent stress was about 133.42 MPa. The reason for the maximum stress value at this position is that the installation of the deep groove ball bearing is close to the shoulder of the lead screw shaft. According to the literature [27], the yield strength of GCr15 material is 518.4 MPa. If the safety factor is 2, the maximum von Mises equivalent stress at the lead screw under working condition C meets the strength requirements, and the maximum allowable stress is not exceeded under other working conditions.

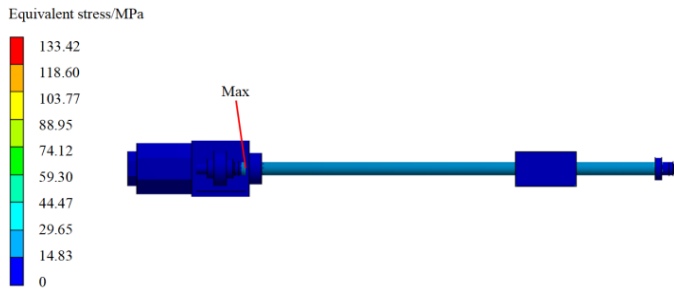


Fig. 7. von Mises equivalent stress distribution contour plot of the screw

4. THERMAL CHARACTERISTIC TEST

This paper mainly conducted the research and analysis of the thermal characteristics of the feed system under the condition of thermal-fluid-solid field coupling. The focus was on obtaining the thermal characteristics such as temperature field distribution, temperature rise, and heat balance time through analysis and establishment of an experimental platform. The comparison results verified the validity of the research content proposed in this paper through comparison with simulation and experiment. As for the mechanical properties of thermal stress and thermal strain, this paper obtains them through finite element simulation analysis and further deduces the consistency of mechanical results according to the effective test results of temperature. Figure 8 demonstrates the hardware components of the experimental platform used for evaluating the thermal characteristics of the CNC machine tool feed system. These components primarily include the magnetic electric resistance temperature sensor (temperature measurement resolution: 0.1°C, measurement accuracy: 0.4°C, measurement range: 0–100°C), the Fluke thermal

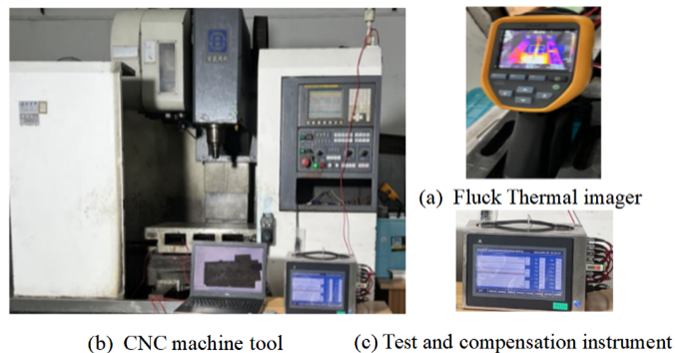


Fig. 8. Numerical control machine tool thermal characteristics test platform

imager (model number: FLUKE TiS50, resolution: 320×240, measurement range: –20–450°C, Thermal sensitivity (NETD): ≤ 0.08°C at 30°C target temperature), the thermal characteristics testing and compensation instrument of the CNC machine tool, and the machine tool body. The purpose of this test platform is to assess and study the thermal behavior exhibited by the feed system in CNC machine tools. The experimental data are analyzed, collected, and processed by using the temperature sensor connected with the thermal characteristic test and compensation instrument of the CNC machine tool. Due to the challenges in placing temperature sensors directly on the ball screw shaft, a thermal imager was chosen to collect temperature data along the screw shaft, and then the image data collected by the thermal imager is analyzed and processed by smart view software.

According to the symmetry of the structure of the guide rail, workbench, bed saddle, and ball screw in the ball screw feed system as well as the thermal sensitive points of the system, 15 measuring points (five on the workbench, three on the bed, two on the guide rail, two on the bearing, one on the screw nut, one on the motor, and one on the ambient temperature) are selected, as shown in Fig. 9. The magnetic thermistor temperature sensor was used in the experiment, and the data sampling interval was 5 s. The temperature measuring points were arranged as shown in Table 9. At the same time, Fluke thermal imager was used to collect experimental data at the lead screw, and the shooting interval was 2 minutes. Measurement duration 3 hours from the start of feed system operation. Let it cool completely before moving on to the next set of experiments. The experiment collected a total of 3000 mm/min feed rate 200 mm stroke, 3000 mm/min feed rate 400 mm stroke, 4000 mm/min feed rate 200 mm stroke, 4000 mm/min feed rate 400 mm stroke, 5000 mm/min feed rate 200 mm stroke, 5000 mm/min feed rate 400 mm stroke, 6000 mm/min feed rate 200 mm stroke and 6000 mm/min feed rate 400 mm stroke experimental data under eight working conditions.

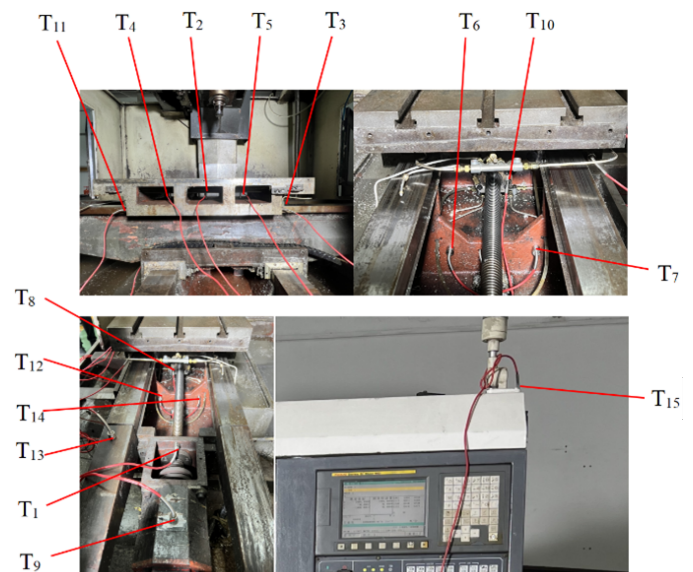


Fig. 9. Layout of temperature measuring points

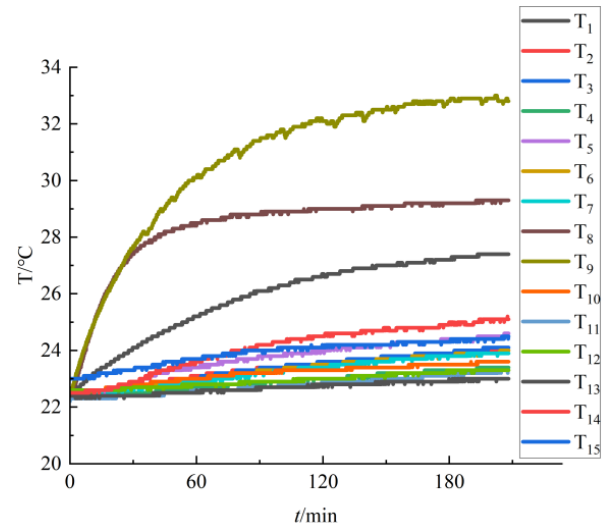
Table 9

Layout of temperature measuring points

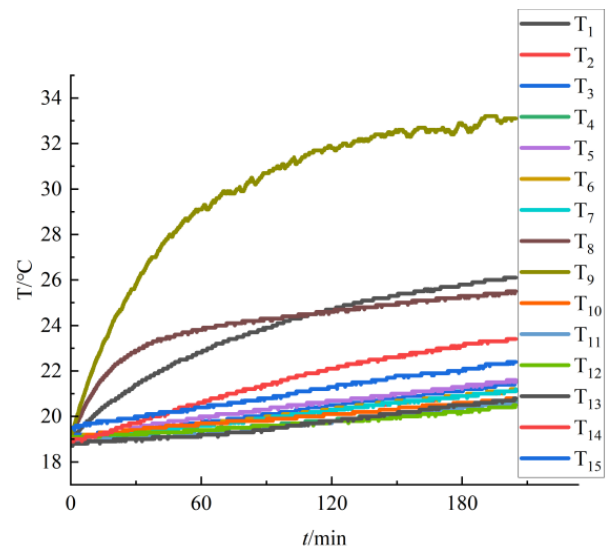
Sensor number	Temperature measuring point location
T ₁	Deep groove ball bearing seat
T ₂	Inside the workbench (middle)
T ₃	The contact between the right side of the workbench and the guide rail
T ₄	Inside the workbench (left)
T ₅	Inside the workbench (right)
T ₆	Bottom left on the right side of the bed
T ₇	Bottom right on the right side of the bed
T ₈	Screw nut
T ₉	Motor housing
T ₁₀	Angular contact ball bearing outer end cap
T ₁₁	The contact between the left side of the workbench and the guide rail
T ₁₂	Bottom left on the left side of the bed
T ₁₃	Left side of the guide rail
T ₁₄	Right side of the guide rail
T ₁₅	Ambient temperature

The experimental data of working condition A: 3000 mm/min feed rate of 200 mm stroke, working condition B: 4000 mm/min feed rate of 200 mm stroke, and working condition C: 6000 mm/min feed rate of 400 mm stroke were selected for analysis. According to the two criteria for determining the thermal balance time of machine tools based on the temperature-time change law and the thermal displacement-time change law in literature [29], when the temperature rise of the machine reaches 95% of the maximum temperature rise, the machine can be considered to be in a state of thermal balance. As shown in Fig. 10, the ball screw system can be considered to have reached a state of thermal balance after 180 minutes.

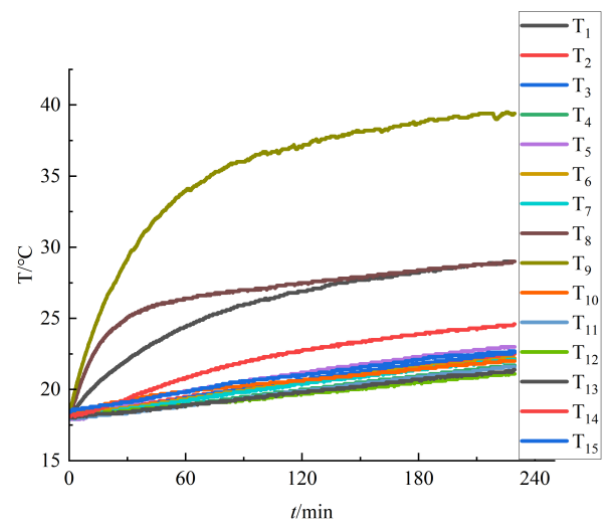
In order to verify the validity of the analysis model, four measuring points (thermal sensitive points) with the most obvious temperature change were selected as the main analysis points according to the simulation results of the temperature field mentioned in the previous section, including one on the screw nut, one on the motor housing, one on the deep groove ball bearing seat, and one on the outer end cover of the angular contact bearing. The experimental data collected by the temperature sensor after the thermal balance is reached are compared with the simulation results of the steady-state temperature field at the corresponding points in the analysis model, as shown in Tables 10–12. The obtained results demonstrate that, under all three operating conditions, there exists an approximate maximum absolute error of 2.4°C and a maximum relative error of 8.7% between the simulated results and experimental data. The comparison between the simulation results and experimental



(a) Working condition A



(b) Working condition B



(c) Working condition C

Fig. 10. Temperature change curve of each measuring point with time

data indicates minimal disparity, suggesting the logical and accurate nature of the multi-physical field analysis model utilized for the feed system.

Table 10

Comparison between simulation results and temperature measuring point experiments (Working condition A)

Sensor point	Experimental data (°C)	Simulation result (°C)	Absolute error (°C)	Relative error
T ₁	32.8	33.5	0.7	2.1%
T ₈	29.3	30.7	1.4	4.8%
T ₉	27.4	29.3	1.9	6.9%
T ₁₀	23.6	25.3	1.7	7.2%

Table 11

Comparison between simulation results and temperature measuring point experiments (Working condition B)

Sensor point	Experimental data (°C)	Simulation result (°C)	Absolute error (°C)	Relative error
T ₁	33.1	33.7	0.6	1.8%
T ₈	25.5	26.8	1.3	5.1%
T ₉	26.1	27.4	1.3	5.0%
T ₁₀	20.8	21.7	0.9	4.3%

Table 12

Comparison between simulation results and temperature measuring point experiments (Working condition C)

Sensor point	Experimental data (°C)	Simulation result (°C)	Absolute error (°C)	Relative error
T ₁	39.4	40.6	1.2	3.0%
T ₈	29.0	30.7	1.7	5.9%
T ₉	29.0	31.4	2.4	8.3%
T ₁₀	22.0	23.9	1.9	8.7%

To ascertain the precision of the temperature field analysis for the lead screw, a comprehensive evaluation was conducted by comparing thermal images captured using a Fluke thermal imager with the simulation results, as depicted in Fig. 11. Six distinct measuring points were selected on the lead screw, namely a thermal sensitive point T16 near the nut, a thermal sensitive point T21 near the right end bearing, and four equidistant measuring points (T17, T18, T19, and T20) positioned between them. The temperature values obtained from both the experimental measurements and the simulation model for each measuring point were meticulously compared. Detailed results for each measuring point can be found in Tables 13–15.

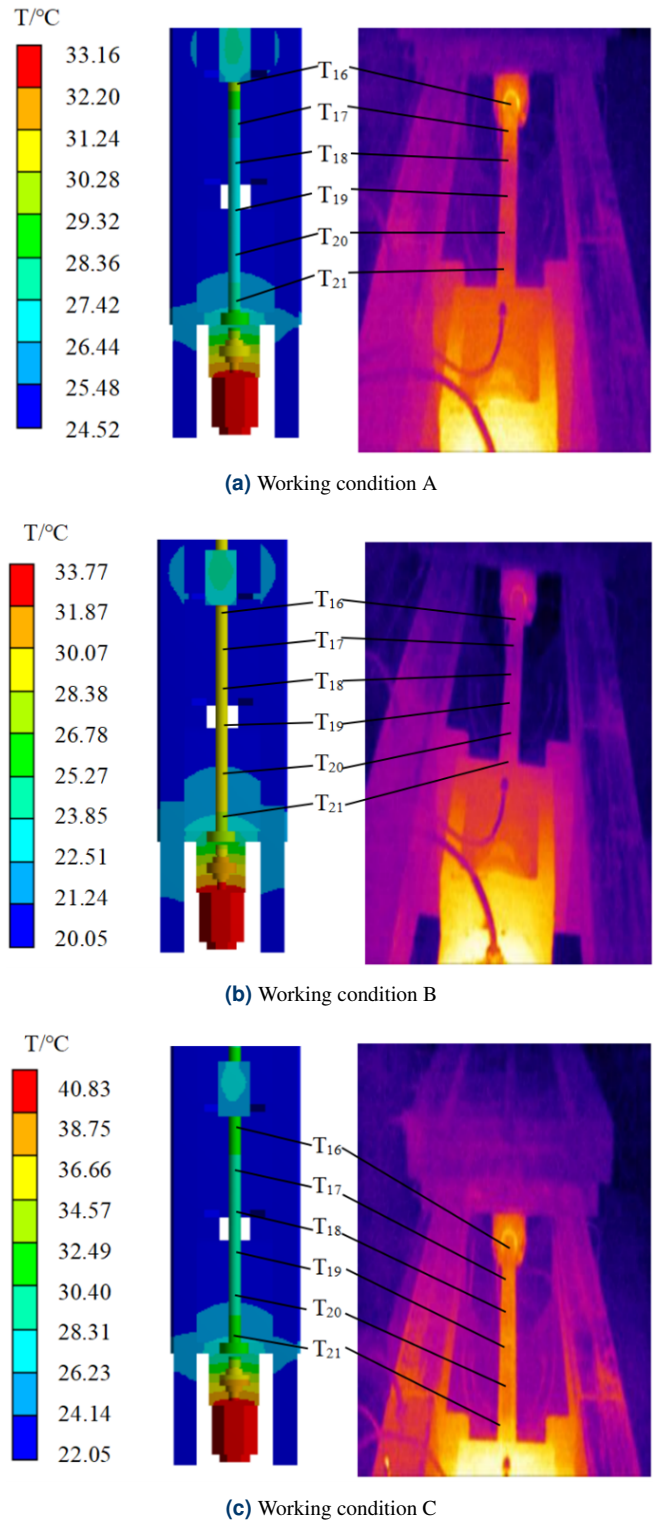


Fig. 11. Comparison of lead screw steady-state simulation analysis and thermal image results

Upon analyzing the comparison results, it is evident that the maximum absolute error and maximum relative error for each measuring point are approximately 2.0°C and 6.8%, respectively. These findings indicate a close agreement between the simulation model analysis results and the measured val-

Table 13

Comparison between simulation results and thermal image temperature data (Working condition A)

Measuring point	Experimental data (°C)	Simulation result (°C)	Absolute error (°C)	Relative error
T ₁₆	30.8	31.7	0.9	2.9%
T ₁₇	29.2	31.2	2.0	6.8%
T ₁₈	29.4	30.9	1.5	5.1%
T ₁₉	29.8	30.6	0.8	2.7%
T ₂₀	29.6	30.3	0.7	2.4%
T ₂₁	29.5	29.8	0.3	1.1%

Table 14

Comparison between simulation results and thermal image temperature data (Working condition B)

Measuring point	Experimental data (°C)	Simulation result (°C)	Absolute error (°C)	Relative error
T ₁₆	27.6	28.3	0.7	2.5%
T ₁₇	27.2	27.7	0.5	1.8%
T ₁₈	26.6	27.5	0.9	3.4%
T ₁₉	26.4	27.3	0.9	3.4%
T ₂₀	26.4	27.2	0.8	3.0%
T ₂₁	28.0	27.1	0.9	3.2%

Table 15

Comparison between simulation results and thermal image temperature data (Working condition C)

Measuring point	Experimental data (°C)	Simulation result (°C)	Absolute error (°C)	Relative error
T ₁₆	30.5	31.2	0.7	2.2%
T ₁₇	30.9	30.2	0.7	2.3%
T ₁₈	31.5	29.8	1.7	5.4%
T ₁₉	30.8	29.8	1.0	3.2%
T ₂₀	30.8	30.1	0.7	2.2%
T ₂₁	31.6	30.6	1.0	3.2%

ues. Thus, affirming the reliability and accuracy of the simulation model in capturing the temperature distribution on the lead screw.

5. CONCLUSION

1. The innovation of this paper lies in the establishment of a multi-physics coupling thermal analysis method for the feed system. The model was developed based on the fundamen-

tal principles of Fourier's law of thermal conductivity and the law of conservation of energy. By simulating the heat transfer between components of the feed system, the convective heat transfer between components and air, and the thermal deformation of the feed system caused by temperature changes, the method calculates and obtains the temperature field, thermal deformation, and thermal stress of each component of the feed system. An experimental platform is built, and the contact measurement and non-contact measurement methods are combined. The thermal characteristic data of the fixed component and the moving component of the machine tool feed system are collected and compared, and the effectiveness of the method is verified.

2. In this study, a dedicated test platform was devised and constructed to examine the thermal traits of CNC machine tools. Temperature data was collected from various components, including the lead screw and ball screw, using thermal imagers and temperature sensors. The results indicate that the maximum absolute error and maximum relative error between the simulated and experimental temperature field outcomes of the feed system are approximately 2.4°C and 8.7%, respectively. This research presents a novel analytical approach to predict the thermal behavior of the ball screw feed system in CNC machine tools, offering a prompt and efficient method to evaluate its thermal characteristics.
3. The feed system of a machine tool experiences a temperature rise during operation due to the influence of multiple physical factors. Apart from the motor, the screw nut exhibits the highest temperature increase. As the temperature changes, the lead screw undergoes significant thermal deformation. Specifically, at a feed rate of 6000 and a stroke of 400, the lead screw can experience a maximum axial thermal deformation of approximately 11.6 μm.

ACKNOWLEDGEMENTS

This research was financially supported by the National Natural Science Foundation of China (52175472), Zhejiang Provincial Natural Foundation of China (LD24E050011; LZYZ21E050002; LGG22E050031), Natural Science Foundation of Zhejiang Province for Distinguished Young Scholars (LR22E050002) and Science and Technology Plan Project of Quzhou (2022K90; 2021K41).

REFERENCES

- [1] B. Man, Y. Guo, X.-Y. Fan, L. Li, and Ch.-X. Li, "Research status and development trend of thermal error of ball screw feed system for machine tool," *Mach. Tool Hydraulics*, vol. 45, no. 15, pp. 174–179, 2021, doi: [10.3969/j.issn.1001-3881.2021.15.035](https://doi.org/10.3969/j.issn.1001-3881.2021.15.035). (in Chinese)
- [2] M. Macko, I. Rojek, M. Sága, T. Burczyński, and D. Mikołajewski, "Machine modelling and simulations," *Bull. Pol. Acad. Sci. Tech. Sci.*, vol. 69, no. 2, p. e136716, 2021, doi: [10.24425/bpasts.2021.136716](https://doi.org/10.24425/bpasts.2021.136716).
- [3] T.-J. Li, C.-Y. Zhao, and Y.-M. Zhang, "Adaptive real-time model on thermal error of ball screw feed drive systems of CNC machine

- tools,” *Int. J. Adv. Manuf. Technol.*, vol. 94, pp. 3853–3861, 2018, doi: [10.1007/s00170-017-1076-5](https://doi.org/10.1007/s00170-017-1076-5).
- [4] J. Yang, C. Li, M. Xu, and Y. Zhang, “Analysis of thermal error model of ball screw feed system based on experimental data,” *Int. J. Adv. Manuf. Technol.*, vol. 119, no. 11, pp. 7415–7427, 2022, doi: [10.1007/s00170-022-08752-w](https://doi.org/10.1007/s00170-022-08752-w).
- [5] C. Ma, J. Yang, X.S. Mei, L. Zhao, H. Shi, and D.S. Zhang, “Dynamic Thermal-Structure Coupling Analysis and Experimental Study on Ball Screw Feed Drive System of Precision Machine Tools,” *Appl. Mech. Mater.*, vol. 868, pp. 124–135, 2017, doi: [10.4028/www.scientific.net/AMM.868.124](https://doi.org/10.4028/www.scientific.net/AMM.868.124).
- [6] J. Xia, Y. Hu, B. Wu, and T. Shi, “Numerical solution, simulation and testing of the thermal dynamic characteristics of ball-screws,” *Front. Mech. Eng. China*, vol. 3, no. 1, pp. 28–36, 2008, doi: [10.1007/s11465-008-0007-4](https://doi.org/10.1007/s11465-008-0007-4).
- [7] R.J. Liang, W.H. Ye, Q.Q. Chen, and X.J. Zhao, “The Thermal Characteristics of the Ball Screw Feed System on a Gantry Machine Tool,” *Appl. Mech. Mater.*, vol. 490–491, pp. 1008–1012, 2014, doi: [10.4028/www.scientific.net/AMM.490-491.1008](https://doi.org/10.4028/www.scientific.net/AMM.490-491.1008).
- [8] D. Su, Y. Li, W. Zhao, and H. Zhang, “Transient thermal error modeling of a ball screw feed system,” *Int. J. Adv. Manuf. Technol.*, vol. 124, no. 7, pp. 2095–2107, 2023, doi: [10.1007/s00170-022-10457-z](https://doi.org/10.1007/s00170-022-10457-z).
- [9] J. Zaplata, “Measurements of temperature of CNC machine tool ball screw utilising IR method,” *Int. J. Appl. Mech.*, vol. 22, no. 3, pp. 769–777, 2017, doi: [10.1515/ijame-2017-0049](https://doi.org/10.1515/ijame-2017-0049).
- [10] T. Li, T. Sun, Y. Zhang, and C. Zhao, “Prediction of thermal error for feed system of machine tools based on random radial basis function neural network,” *Int. J. Adv. Manuf. Technol.*, vol. 114, no. 5, pp. 1545–1553, 2021, doi: [10.1007/s00170-021-06899-6](https://doi.org/10.1007/s00170-021-06899-6).
- [11] X.-L. Deng, *et al.*, “Multi-source heterogeneous information acquiring test experiment and platform construction for CNC machine tool,” *Opt. Precis. Eng.*, vol. 30, no. 12, pp. 1440–1451, 2022, doi: [10.37188/OPE.20223012.1440](https://doi.org/10.37188/OPE.20223012.1440). (in Chinese)
- [12] X.-L. Deng, *et al.*, “Temperature measurement point selection method of multi-machine tool based on weighted fusion matrix system clustering,” *J. Zhejiang Univ. Eng. Sci.*, vol. 57, no. 6, pp. 1147–1156, 2023, doi: [10.3785/j.issn.1008-973X.2023.06.010](https://doi.org/10.3785/j.issn.1008-973X.2023.06.010). (in Chinese)
- [13] A. Oyanguren, J. Larranaga, and I. Ulacia, “Thermo-mechanical modelling of ball screw preload force variation in different working conditions,” *Int. J. Adv. Manuf. Technol.*, vol. 97, pp. 723–739, 2018, doi: [10.1007/s00170-018-2008-8](https://doi.org/10.1007/s00170-018-2008-8).
- [14] H. Shi, C. Ma, and J. Yang, “Investigation into effect of thermal expansion on thermally induced error of ball screw feed drive system of precision machine tools,” *Int. J. Mach. Tools Manuf.*, vol. 97, pp. 60–71, 2015, doi: [10.1016/j.ijmactools.2015.07.003](https://doi.org/10.1016/j.ijmactools.2015.07.003).
- [15] Z.-Z. Xu, C. Choi, L. Liang, D. Li, and S.-K. Lyu, “Study on a novel thermal error compensation system for high-precision ball screw feed drive (1st report: Model, calculation and simulation),” *Int. J. Precis. Eng. Manuf.*, vol. 16, no. 9, pp. 2005–2011, 2015, doi: [10.1007/s12541-015-0261-4](https://doi.org/10.1007/s12541-015-0261-4).
- [16] X. Min and S. Jiang, “A thermal model of a ball screw feed drive system for a machine tool,” *J. Mech. Eng. Sci.*, vol. 255, pp. 187–193, 2011, doi: [10.1243/09544062JMES2148](https://doi.org/10.1243/09544062JMES2148).
- [17] Z.-H. Li, K.-G. Fan, and Y. Zhan, “Time-varying positioning error modeling and compensation for ball screw systems based on simulation and experiment analysis,” *Int. J. Adv. Manuf. Technol.*, vol. 73, pp. 773–782, 2014, doi: [10.1007/s00170-014-5865-9](https://doi.org/10.1007/s00170-014-5865-9).
- [18] X.-L. Deng *et al.*, “Thermal characteristics analysis and test of spindle-column system for CNC machine tool,” *Opt. Precis. Eng.*, vol. 28, no. 3, pp. 601–609, 2020, doi: [10.3788/OPE.20202803.0601](https://doi.org/10.3788/OPE.20202803.0601). (in Chinese)
- [19] H. Lamb, *Hydrodynamics*. Beijing, World Book Publishing Company, 2015.
- [20] S.-M. Yang and W.-X. Tao, *Thermal transfer*. Beijing, Higher Education Press, 2006.
- [21] A. Verl and S. Frey, “Correlation between feed velocity and preloading in ball screw drive,” *CIRP Ann. Manuf. Technol.*, vol. 59, pp. 429–432, 2010, doi: [10.1016/j.cirp.2010.03.136](https://doi.org/10.1016/j.cirp.2010.03.136).
- [22] J. Yang, D. Zhang, X. Mei, L. Zhao, C. Ma, and H. Shi, “Thermal error simulation and compensation in a jig-boring machine equipped with a dual-drive servo feed system,” *Proc. Inst. Mech. Eng. Part B J. Eng. Manuf.*, vol. 229, no. 1_suppl, pp. 43–63, Nov. 2014, doi: [10.1177/0954405414555592](https://doi.org/10.1177/0954405414555592).
- [23] M. Gebhardt, J. Mayr, N. Furrer, T. Widmer, S. Weikert, and W. Knapp, “High precision grey-box model for compensation of thermal errors on five-axis machines,” *CIRP Ann.*, vol. 63, no. 1, pp. 509–512, 2014, doi: [10.1016/j.cirp.2014.03.029](https://doi.org/10.1016/j.cirp.2014.03.029).
- [24] X.-L. Deng, J.-Z. Fu, Y. He, and Z.-Ch. Chen, “Multi-field coupling thermal characteristics analysis for spindle system of precision CNC machine tool,” *J. Zhejiang Univ. Eng. Sci.*, vol. 47, no. 10, pp. 1863–1870, 2013, doi: [10.3785/j.issn.1008-973X.2013.10.024](https://doi.org/10.3785/j.issn.1008-973X.2013.10.024). (in Chinese)
- [25] W.-T. Li, B.-H. Huang, and Z.-B. Bi, *Theoretical analysis and application of thermal stress*, Beijing: China Electric Power Press, 2004.
- [26] P. Yin, Y.-H. Zheng, and X.-C. Qing, “Finite element analysis of precision CNC machine tool feed system,” *Digital Manuf. Sci.*, vol. 20, no. 1, pp. 39–44, 2022, doi: [10.3963/j.issn.1672-3236.2022.01.008](https://doi.org/10.3963/j.issn.1672-3236.2022.01.008). (in Chinese)
- [27] D.-X. Cheng, *Mechanical Design Manual*. Beijing, Publishing House of Electronics Industry, 2007.
- [28] X.-H. Xu, G.-P. Jiang, X.-G. Han, and Z.-P. Zhang, “Analysis and Calculation of Comprehensive Axial Deformations of Ball Screw-Bearing in Ball Screw Support Units,” *China Mech. Eng.*, vol. 34, no. 7, pp. 830–837, 2023, doi: [10.3969/j.issn.1004-132X.2023.07.009](https://doi.org/10.3969/j.issn.1004-132X.2023.07.009). (in Chinese)
- [29] X.-L. Deng, J.-Z. Fu, H.-Y. Shen, and Z.-Ch. Chen, “Thermal equilibrium test for multi spindle system of precision CNC machine tool,” *J. Zhejiang Univ. Eng. Sci.*, vol. 48, no. 9, pp. 1645–1653, 2014, doi: [10.3785/j.issn.1008-973X.2014.09.015](https://doi.org/10.3785/j.issn.1008-973X.2014.09.015). (in Chinese)